

Differential interference theory of vortex beam at interface reflection

WANG Liang, YANG Qiang, TANG Long-tao, WEN Shuang-chun, LUO Hai-lu

Citation:

WANG Liang, YANG Qiang, TANG Long-tao, WEN Shuang-chun, LUO Hai-lu. Differential interference theory of vortex beam at interface reflection[J]. *Chinese Optics*, In press. doi: 10.37188/CO.EN-2026-0010

王亮, 杨强, 唐龙涛, 文双春, 罗海陆. 涡旋光束在界面反射的微分干涉理论[J]. *中国光学*, 优先发表. doi: 10.37188/CO.EN-2026-0010

View online: <https://doi.org/10.37188/CO.EN-2026-0010>

Articles you may be interested in

[Measurement of orbital angular momentum of vortex beam by topological charge difference](#)

涡旋光轨道角动量的拓扑荷差值法测量

Chinese Optics. 2025, 18(2): 216 <https://doi.org/10.37188/CO.2024-0141>

[The Poynting vectors, spin and orbital angular momentums of uniformly polarized cosh-Pearcey-Gauss beams in the far zone](#)

均匀偏振cosh-Pearcey-Gauss光束的远场坡印廷矢量, 自旋与轨道角动量

Chinese Optics. 2023, 16(5): 1195 <https://doi.org/10.37188/CO.EN.2022-0022>

[Recognition method for vortex beams orbital angular momentum with imbalanced label](#)

标签分布不平衡的涡旋光束轨道角动量识别

Chinese Optics. 2025, 18(2): 207 <https://doi.org/10.37188/CO.2024-0155>

[Orbital-angular-momentum spectra in coherent optical vortex beam arrays with hybrid states of polarization](#)

杂化偏振涡旋合成光束阵列的轨道角动量谱

Chinese Optics. 2023, 16(6): 1501 <https://doi.org/10.37188/CO.EN-2023-0010>

[Crosshair detection method for orbital angular momentum of vortex beams](#)

涡旋光束轨道角动量的十字线检测法

Chinese Optics. 2025, 18(4): 803 <https://doi.org/10.37188/CO.2024-0209>

[Scintillation index analysis of radial Gaussian vortex beam array propagation in the atmosphere](#)

径向高斯涡旋光束阵列在大气中传输的闪烁指数分析

Chinese Optics. 2025, 18(1): 142 <https://doi.org/10.37188/CO.2024-0098>

文章编号 2097-1842(xxxx)x-0001-10

Differential interference theory of vortex beam at interface reflection

WANG Liang, YANG Qiang, TANG Long-tao, WEN Shuang-chun, LUO Hai-lu*
(Laboratory for Spin Photonics, School of Physics and Electronics, Hunan University,
Changsha 410082, China)

* Corresponding author, E-mail: hailuluo@hnu.edu.cn

Abstract: Weak measurement technique based on weak-value amplification offers an effective method to detect the tiny spin splitting in the photonic spin Hall effect. However, its performance is constrained under conditions of strong coupling or near-orthogonality between the pre- and post-selected states. Based on differential interference theory, this work establishes a relation between the spin-dependent displacement and the amplified displacement for vortex beam with arbitrary topological charge under partial reflection at an air-glass interface. The relation remains valid even under strong-coupling conditions or when the pre- and post-selected states are nearly orthogonal, and is applicable for arbitrary incident linear polarizations. The corresponding characteristics of vortex beam reflected at an air-glass interface is systematically analyzed, and the influences of key parameters including the incident angle, topological charge, incident polarization state, post-selection angle, and propagation distance on the amplified displacement are elucidated. This study provides a valuable theoretical foundation for the applications of vortex beam in precision optical measurement and optical micromanipulation.

Key words: differential interference; weak measurement; OAM beam; the photonic spin Hall effect

涡旋光束在界面反射的微分干涉理论

王亮, 杨强, 唐龙涛, 文双春, 罗海陆*
(湖南大学物理与微电子科学学院自旋光子学实验室, 湖南长沙 410082)

摘要: 基于弱值放大的弱测量技术为探测光子自旋霍尔效应中的微小自旋分裂提供了一种有效方法。然而, 在强耦合或前选择和后选择近乎正交的条件下, 其性能受到限制。本文基于微分干涉理论, 建立了携带任意拓扑荷的涡旋光束在空气-玻璃界面部分反射下的自旋相关位移与放大位移之间的关系。该关系即使在强耦合条件下或前选择和后选择近乎正交时仍然有效, 并且适用于任意入射线偏振态。本文系统分析了涡旋光束在空气-玻璃界面反射的特性, 并阐明了入射角、拓扑荷、入射偏振态、后选择角和传播距离等关键参数对放大位移的影响。这项研究为涡旋光束在精密光学测量和光学微操控中的应用提供了重要的理论基础。

关键词: 微分干涉; 弱测量; 轨道角动量光束; 光子自旋霍尔效应

中图分类号: O436.1

文献标志码: A

doi: 10.37188/CO.EN-2026-0010

CSTR: 32171.14.CO.EN-2026-0010

收稿日期: 2026-03-31; 修订日期: xxxx-xx-xx

基金项目: 国家自然科学基金(No. 12174097)资助

Supported by National Natural Science Foundation of China (No. 12174097)

1 Introduction

The photonic spin Hall effect (PSHE) refers to the tiny splitting of left- and right-handed circular polarization components in a light beam upon reflection or refraction, caused by spin-orbit coupling^[1-5]. This effect provides a powerful platform for studying fundamental spin-orbit interactions in photonics and offers promising applications in nanophotonics^[6-8], phase reconstruction^[9-10], and image processing^[11-13]. However, the magnitude of this spin-dependent displacement is typically at the sub-wavelength scale, posing a significant challenge for direct experimental detection.

Weak measurement provides a feasible method for accurately amplifying and measuring this tiny displacement, relying on the critical condition that the probe wave function remains almost undisturbed during the measurement procedure^[14]. However, this condition is often not satisfied in some practical scenarios, such as in the strong-coupling regime or when the pre-selected and post-selected states are nearly orthogonal. To overcome these limitations, a modified weak measurement scheme has been proposed^[15], but it introduces an ambiguity in the definition of the weak value. The weak value in standard weak measurement is well-defined, as it can be directly computed from the pre-selected and post-selected states of the system and the system's observable operator. By contrast, the weak value in the modified weak measurement scheme is obtained from the ratio of the amplified displacement to the initial displacement. This approach adapts the measurement model to fit specific scenarios without refining the definition of the weak value under failure conditions, making it impossible to interpret the formation mechanism of the amplified displacement from the weak-value perspective.

Notably, vortex beams possess intrinsic orbital angular momentum (IOAM)^[16], a fundamental feature that distinguishes them from Gaussian beams

and endows them with unique advantages in exploring spin-orbit coupling. Despite the great significance of detecting the PSHE in vortex beams, such studies either continue to adopt weak measurement methods or only focus on polarization in one specific direction^[17]. In fact, the detection of the PSHE with arbitrary linearly polarized states also requires a modified model. In this work, we propose a differential interference scheme for detecting the PSHE of vortex beams, which effectively overcomes the limitations of weak measurement and is applicable to all incident polarization states. Based on this scheme, we rederive the relation between the spin-dependent displacement and the amplified displacement, verify that the pre- and post-selection measurement protocol remains valid even when weak measurement breaks down, and clarify the formation mechanism of the amplified displacement.

2 Theoretical formulations

This section is devoted to a theoretical model for detecting tiny displacements using differential interference. We consider a Laguerre-Gaussian beam undergoing partial reflection at an air-glass interface, as shown in Fig. 1. The angular spectrum of an arbitrarily linearly polarized Laguerre-Gaussian beam with radial index $p = 0$ is formulated as

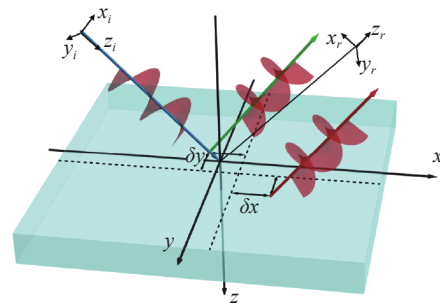


Fig. 1 A schematic diagram of the transverse δ_y and longitudinal δ_x spin splitting of an arbitrary linearly polarized Laguerre-Gaussian beam incident on an interface. Solid green and red lines indicate the left-handed and right-handed circularly polarized components in the reflected light, respectively, and dashed lines represent spin-independent global displacements.

$$\tilde{\mathbf{E}}_i(k_{ix}, k_{iy}) = N_l [-ik_{ix} + \text{sign}(l)k_{iy}]^{|l|} \times \exp\left[-\frac{z_R(k_{ix}^2 + k_{iy}^2)}{2k_0}\right] \begin{bmatrix} \cos\alpha_i \\ \sin\alpha_i \end{bmatrix}, \quad (1)$$

where $N_l = w_0^{|l|+1} / \sqrt{2^{|l|-1}\pi|l|!}$ is the normalization constant. l is topological charge, w_0 is the beam waist radius, $z_R = \pi w_0^2 / \lambda$ is the Rayleigh range, k_0 is the wave number of the incident beam in vacuum, and α_i denotes the polarization angle.

After the beam is reflected at the interface, the transformation of the angular spectrum can be described by the reflection matrix, which is given by^[18]

$$\mathbf{R} = \begin{bmatrix} r_p + \frac{k_{ix}}{k_0} r_p' & \frac{k_{iy}}{k_0} (r_p + r_s) \cot\theta_i \\ -\frac{k_{iy}}{k_0} (r_p + r_s) \cot\theta_i & r_s + \frac{k_{ix}}{k_0} r_s' \end{bmatrix}, \quad (2)$$

where r_p and r_s are the Fresnel reflection coefficients for p - and s -polarization, θ_i is the incidence angle, $r_p' = \partial r_p / \partial \theta_i$ and $r_s' = \partial r_s / \partial \theta_i$, k_{ix} and k_{iy} are the transverse numbers. Hence, the angular spectrum of the reflected beam is

$$\tilde{\mathbf{E}}_r(k_{rx}, k_{ry}) = \mathbf{R} \cdot \tilde{\mathbf{E}}_i(k_{ix}, k_{iy}) = \begin{bmatrix} (1 - k_{rx}\Delta_H) r_p \cos\alpha_i + k_{ry}\delta_V r_s \sin\alpha_i \\ k_{ry}\delta_H r_p \cos\alpha_i + (1 - k_{rx}\Delta_V) r_s \sin\alpha_i \end{bmatrix} \times N_l \exp\left[-\frac{z_R(k_{rx}^2 + k_{ry}^2)}{2k_0}\right] \times [ik_{rx} + \text{sign}(l)k_{ry}]^{|l|}, \quad (3)$$

in which the boundary conditions $k_{rx} = -k_{ix}$, $k_{ry} = k_{iy}$ have been used, and $\Delta_H = (\partial \ln r_p) / (k_0 \partial \theta_i)$, $\Delta_V = (\partial \ln r_s) / (k_0 \partial \theta_i)$, $\delta_H = (r_p + r_s) \cot\theta_i / (k_0 r_p)$, $\delta_V = (r_p + r_s) \cot\theta_i / (k_0 r_s)$.

Under the paraxial approximation, inverse Fourier transformation gives the reflected field

$$f(x_r, y_r, z_r) = \sqrt{\frac{2}{\pi|l|!}} \frac{z_R}{w(z_R + iz_r)} \times \exp\left[-\frac{k_0(x_r^2 + y_r^2)}{2(z_R + iz_r)}\right] \times \left\{ \frac{\sqrt{2}iz_R [ix_r + \text{sgn}(l)y_r]}{w_0(z_R + iz_r)} \right\}^{|l|}, \quad (4)$$

$$\mathbf{E}_r^H(x_r, y_r, z_r) = \begin{bmatrix} r_p \cos\alpha_i \left(f + i\Delta_H \frac{\partial f}{\partial x_r} \right) - ir_s \delta_V \sin\alpha_i \frac{\partial f}{\partial y_r} \\ \end{bmatrix} \mathbf{e}_x, \quad (5)$$

$$\mathbf{E}_r^V(x_r, y_r, z_r) = \begin{bmatrix} r_s \sin\alpha_i \left(f + i\Delta_V \frac{\partial f}{\partial x_r} \right) + ir_p \delta_H \cos\alpha_i \frac{\partial f}{\partial y_r} \\ \end{bmatrix} \mathbf{e}_y, \quad (6)$$

Here z_r is the propagation distance. In the spin space, we have $\mathbf{e}_x = (\mathbf{e}_+ + \mathbf{e}_-) / \sqrt{2}$ and $\mathbf{e}_y = i(\mathbf{e}_- - \mathbf{e}_+) / \sqrt{2}$. Thus,

$$\mathbf{E}_{r\pm}(x_r, y_r, z_r) = \frac{1}{\sqrt{2}} \left[f(r_p \cos\alpha_i \mp ir_s \sin\alpha_i) + \frac{\partial f}{\partial x_r} (ir_p \Delta_H \cos\alpha_i \pm r_s \Delta_V \sin\alpha_i) + \frac{\partial f}{\partial y_r} (-ir_s \delta_V \sin\alpha_i \pm r_p \delta_H \cos\alpha_i) \right] \mathbf{e}_{\pm}, \quad (7)$$

For each circular polarization component, the initial displacement of the beam centroid is given by

$$\Delta \mathbf{r} = \frac{\iint \mathbf{r} |\mathbf{E}_{r\pm}(x_r, y_r, z_r)|^2 dx_r dy_r}{\iint |\mathbf{E}_{r\pm}(x_r, y_r, z_r)|^2 dx_r dy_r}, \quad (8)$$

where $\mathbf{r} = (x_r, y_r)$. The results of the calculation are

$$\Delta x_r = \frac{-l\vartheta_y + \sigma\delta_x - \frac{z_r}{z_R}(1+|l|)\vartheta_x}{1+D_0}, \quad (9)$$

$$\Delta y_r = \frac{-l\vartheta_x - \sigma\delta_y + \frac{z_r}{z_R}(1+|l|)\vartheta_y}{1+D_0}, \quad (10)$$

in which

$$\vartheta_x = \frac{r_p^2 \Delta_H + r_s^2 \Delta_V \tan^2 \alpha_i}{r_p^2 + r_s^2 \tan^2 \alpha_i}, \vartheta_y = \frac{r_p r_s (\delta_V - \delta_H) \tan \alpha_i}{r_p^2 + r_s^2 \tan^2 \alpha_i},$$

$$\delta_x = \frac{r_p r_s (\Delta_H - \Delta_V) \tan \alpha_i}{r_p^2 + r_s^2 \tan^2 \alpha_i}, \delta_y = \frac{r_p^2 \delta_H + r_s^2 \delta_V \tan^2 \alpha_i}{r_p^2 + r_s^2 \tan^2 \alpha_i},$$

$$D_0 = \frac{1+|l|}{w_0^2} \frac{r_p^2 (\Delta_H^2 + \delta_H^2) + r_s^2 (\Delta_V^2 + \delta_V^2) \tan^2 \alpha_i}{r_p^2 + r_s^2 \tan^2 \alpha_i}.$$

where $\sigma = +1$ and $\sigma = -1$ correspond to the left- and right-handed circular polarization, respectively. When θ_i is far from the Brewster angle θ_B , leading

to $(\Delta_H^2 + \delta_H^2) \ll w_0^2$, we get $D_0 \ll 1$, hence D_0 can be neglected. However, for vortex beam with large topological charge, D_0 may become non-negligible even when θ_i is far from θ_B . The displacement $\sigma\delta_x$ and $\sigma\delta_y$, marked by σ originates from spin-orbit interaction, and the displacement $l\vartheta_y$, $l\vartheta_x$ marked by l arises from orbit-orbit interaction, which is referred to as the orbit-orbit Hall effect^[19-20]. The topological charge l couples the displacements in the two directions, with a coupling strength dependent on l . We focus mainly on the spin-dependent displacements and set $\Delta x_r^{\sigma,l} = \sigma\delta_x / (1 + D_0)$, $\Delta y_r^{\sigma,l} = -\sigma\delta_y / (1 + D_0)$.

The reflected optical field is decomposed into orthogonally polarized horizontal and vertical components, \mathbf{E}_r^H and \mathbf{E}_r^V , as given by Eq. (5) and Eq. (6), respectively. Then, we project \mathbf{E}_r^H and \mathbf{E}_r^V onto a linear polarization axis at an angle β relative to the x_r -axis. The output electric field is thus expressed as

$$\mathbf{E}_{\text{out}} = \mathbf{E}_{x'} + \mathbf{E}_{y'} = \cos\beta\mathbf{E}_r^H + \sin\beta\mathbf{E}_r^V. \quad (11)$$

The projection angle β is set to be nearly orthogonal to the polarization direction of the reflected field, i.e., $\beta = \gamma + \pi/2 + \varepsilon$, where $\gamma = \arctan(r_s / r_p \tan\alpha_i)$ denotes the polarization angle of the reflected field and ε is post-selection angle. The corresponding light intensity distribution is given by $I_{\text{out}} = |\mathbf{E}_{\text{out}}|^2$, from which the beam centroid position can be derived as

$$\langle r \rangle = \frac{\iint r I_{\text{out}}(x, y) dx dy}{\iint I_{\text{out}}(x, y) dx dy}, \quad (12)$$

where $r = (x, y)$. The amplified displacements can be expressed as

$$\langle x \rangle = \frac{l \text{Re}(C^* A) - \text{Im}(B^* A) - \frac{z_r}{z_R} (1 + |l|) \text{Re}(B^* A)}{|A|^2 + \frac{1 + |l|}{w_0^2} (|B|^2 + |C|^2)}, \quad (13)$$

$$\langle y \rangle = \frac{-l \text{Re}(B^* A) - \text{Im}(C^* A) - \frac{z_r}{z_R} (1 + |l|) \text{Re}(C^* A)}{|A|^2 + \frac{1 + |l|}{w_0^2} (|B|^2 + |C|^2)}, \quad (14)$$

where

$$\begin{aligned} A &= r_p \cos\alpha \cos\beta + r_s \sin\alpha \sin\beta, \\ B &= r_p \Delta_H \cos\alpha \cos\beta + r_s \Delta_V \sin\alpha \sin\beta, \\ C &= r_p \delta_H \cos\alpha \sin\beta - r_s \delta_V \sin\alpha \cos\beta. \end{aligned}$$

The above amplified displacements are derived for the general case, applicable to both total internal reflection and partial reflection. For anisotropic interfaces, such as those coated with two-dimensional materials, the differential interference framework remains applicable provided that appropriate reflection coefficients are adopted. In partial reflection, where the Fresnel reflection coefficients are real, Eq. (13) reduces to

$$\langle x \rangle_{\text{PR}} = -\frac{l(\delta_y \cot\varepsilon + \vartheta_y) + \frac{z_r}{z_R} (1 + |l|)(\delta_x \cot\varepsilon + \vartheta_x)}{1 + D_1}, \quad (15)$$

$$\langle y \rangle_{\text{PR}} = -\frac{l(\delta_x \cot\varepsilon + \vartheta_x) - \frac{z_r}{z_R} (1 + |l|)(\delta_y \cot\varepsilon + \vartheta_y)}{1 + D_1}, \quad (16)$$

where

$$D_1 = \frac{1 + |l|}{w_0^2} [(\delta_y \cot\varepsilon + \vartheta_y)^2 + (\delta_x \cot\varepsilon + \vartheta_x)^2],$$

Similarly, when θ_i is far from θ_B and ε is not too small, D_1 can be neglected, and Eq. (13) reduces to the conventional weak measurement formula. Note, however, that for large l , D_1 may become significant, in which case the full denominator should be retained. In comparison with Eq. (9), only the initial spin-dependent displacements are amplified, while the topological charge l also induces coupling between the initial spin-dependent displacements, with the coupling strength proportional to l . If we only consider the incident Gaussian beam with $\alpha_i = 0^\circ$ or $\alpha_i = 90^\circ$, and we can obtain zero longitudinal displacement amplification, which is consistent with the previous results a certain extent^[21]. When $l \neq 0$, due to the coupling between longitudinal and transverse displacements, longitudinal displacement amplification is achieved even for incident beam with horizontal or vertical polarization.

To clearly illustrate the formation mechanism of the amplified displacements, we consider a representative case with $l = 1$, $\alpha_i = 0^\circ$, $\theta_i = 45^\circ$, and $\varepsilon = 1^\circ$, and perform calculations with the observation plane set at $z_r = 2z_R$. The normalized intensities of E_x' and E_y' are displayed in Figs. 2(a) and 2(b), respectively, and their phase distributions are shown in Figs. 2(d) and 2(e). The E_y' arises as an orthogonal polarization state component generated by interface reflection of the finite beam, which is then isolated through polarization post-selection. The phase difference between them is presented in

Fig. 2(f). It is nearly zero for $y < 0$, leading to constructive interference, and approaches $\pm\pi$ for $y > 0$, leading to destructive interference, which ultimately producing the asymmetric intensity distribution shown in Fig. 2(c). In essence, interface reflection causes a slight relative spatial shift between the two orthogonal polarization components. When the reflected beam passes through a polarizer, these components interfere, converting the tiny spatial shift into an intensity imbalance across the beam profile, which manifests as an amplified centroid displacement.

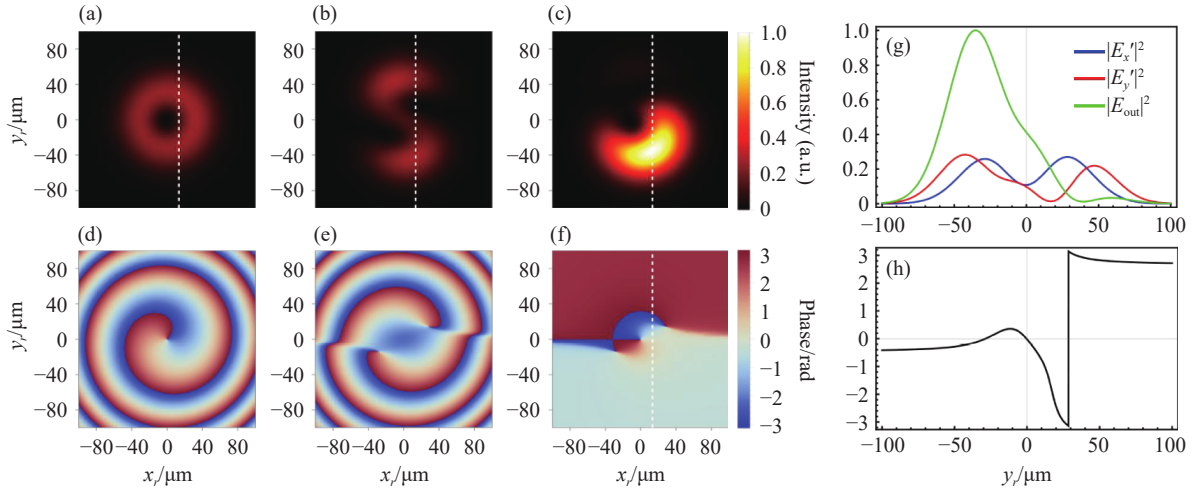


Fig. 2 Differential interference diagram with $l = 1$, $\alpha_i = 0^\circ$, $\theta_i = 45^\circ$, $z_r = 2z_R$, and $\varepsilon = 1^\circ$. (a), (b) Normalized intensity of E_x' and E_y' , respectively. (c) Normalized intensity after interference between E_x' and E_y' . (d) (e) Phase distributions of E_x' and E_y' , respectively. (f) Phase difference between E_x' and E_y' . (g) Normalized intensity along the white dashed lines in (a), (b), and (c). (h) Phase distributions along the white dashed lines in (f).

3 Numerical results and Discussion

A vortex beam is incident from air onto a glass substrate with a refractive index of $n = 1.515$, leading to Brewster angle $\theta_B = 56.5^\circ$. Besides the parameters given at every figure, the common parameters are set as the wavelength $\lambda_0 = 632.8$ nm and the beam waist radius $w_0 = 20$ μm.

We validate the proposed model by calculating the interference-amplified displacement under different parameter configurations. First, we fix $\varepsilon = 1^\circ$ and perform a full scan of θ_i and α_i (each ranging from 0° – 90°). For small α_i , the p -polarized com-

ponent dominates, and both the longitudinal and transverse displacements reverse sign across θ_B and attain an extremum nearby. The calculated longitudinal and transverse amplified displacements are shown in Figs. 3(a) and 3(b), respectively. This behavior arises because, even at θ_B where $r_p = 0$, $\partial r_p / \partial \theta$ remains substantial. As α_i increases, the s -polarized component grows, and the sign reversal and extremum feature gradually weakens. Second, we test the model in the regime where pre-selected and post-selected states approach orthogonality, another scenario where conventional weak measurement is ineffective. We fix $\theta_i = 45^\circ$, vary ε from -2° – 2° , and sweep α_i from 0° – 90° [Figs. 3(c), 3(d)].

Third, we conduct a complementary simulation for the near-orthogonal regime: we fix $\alpha_i = 0^\circ$, vary ε from -2° – 2° , and sweep θ_i from 0° – 90° [Figs. 3(e),

3(f)]. These results demonstrate that the differential interference model remains effective in the key regimes where conventional weak measurement fails.

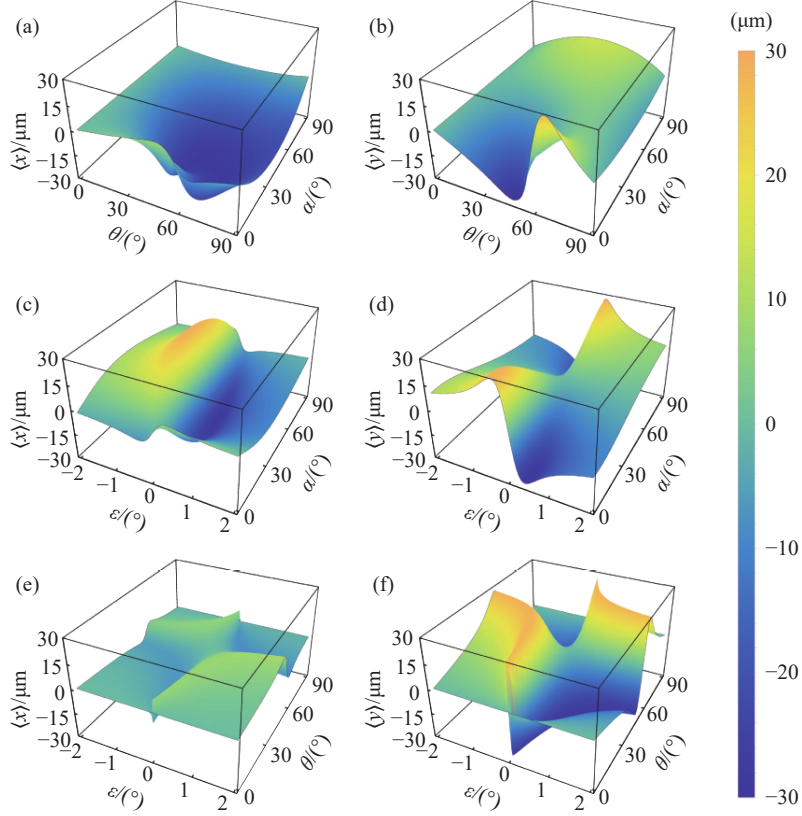


Fig. 3 Amplified displacement for $l = 1$ at $z_r = 2z_R$: (a), (b) with $\varepsilon = 1^\circ$ fixed; (c), (d) with $\theta = 45^\circ$ fixed; (e), (f) with $\alpha_i = 0^\circ$ fixed, in each pair, the x_r - and y_r -direction results are shown in the left and right panels, respectively.

Next, we investigate how the topological charge affects the amplified displacement. Two cases are considered: $\delta_x = 0$ or $\delta_y = 0$, and $\delta_x \neq 0$, $\delta_y \neq 0$. For horizontally polarized incident light, $\delta_x = 0$. Eq. (13) can be simplified as

$$\langle x \rangle_H = -\frac{l\delta_H \cot \varepsilon + \frac{z_r}{z_R}(1+|l|)\Delta_H}{1+D_2}, \quad (17)$$

$$\langle y \rangle_H = -\frac{l\Delta_H - \frac{z_r}{z_R}(1+|l|)\delta_H \cot \varepsilon}{1+D_2}, \quad (18)$$

where

$$D_2 = \frac{1+|l|}{w_0^2}(\Delta_H^2 + \delta_H^2 \cot^2 \varepsilon).$$

Fig. 4(a) and 4(b) depict the dependence of the initial transverse spin-dependent displacement on θ_i

for different topological charges $l = 0, \pm 1, \pm 3$. This displacement depends on $|l|$. When θ_i is far from the θ_B , the D_0 term is negligible, and the effect of $|l|$ remains insignificant. In contrast, near θ_B , however, D_0 becomes substantial and scales with $1+|l|$, reducing the magnitude of the initial transverse displacement as $|l|$ increases. Fig. 4(c) and 4(d) show the amplified longitudinal and transverse displacements at $z_r = 2z_R$ with $\varepsilon = 1^\circ$. Fig. 4(e) presents the intensity distributions at $\theta_i = 30^\circ, 45^\circ$, and 60° , where the longitudinal and transverse amplified displacements are clearly distinguishable. With increasing propagation distance, however, $(z_r/z_R)(1+|l|)\Delta_H$ gradually dominates the longitudinal amplified displacement, while $l\delta_H \cot \varepsilon$ does not increase with propagation. This ultimately results in $\langle y \rangle_H \gg \langle x \rangle_H$, meaning the observed beam centroid displacement

is predominantly transverse. Fig. 5 shows the amplified displacement as a function of θ_i at $z_r = 10z_R$, together with the intensity distributions at $\theta_i = 30^\circ$, 45° , and 60° . Notably, for p -polarized light and $z_r = \text{constant}$, the influence of $|l|$ on the amplified displacement weakens as θ_i approaches θ_B . This occurs because D_2 becomes non-negligible near θ_B , canceling the $1 + |l|$ factor in the numerator. We further

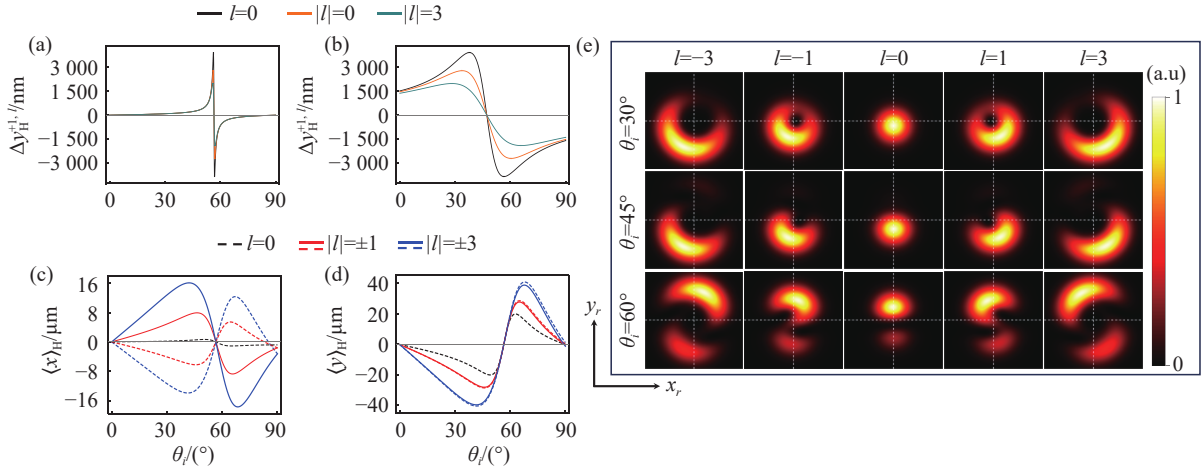


Fig. 4 Initial and amplified displacements for vortex beams with $\alpha_i = 0^\circ$ and $l = 0, \pm 1, \pm 3$, calculated at $z_r = 2z_R$ and $\varepsilon = 0.1^\circ$. (a), (b) Transverse initial displacement (left-handed component) versus θ_i , respectively. (c), (d) Longitudinal and transverse amplified displacements versus θ_i , respectively. (e) Intensity distributions for $\theta_i = 30^\circ, 45^\circ$, and 60° .

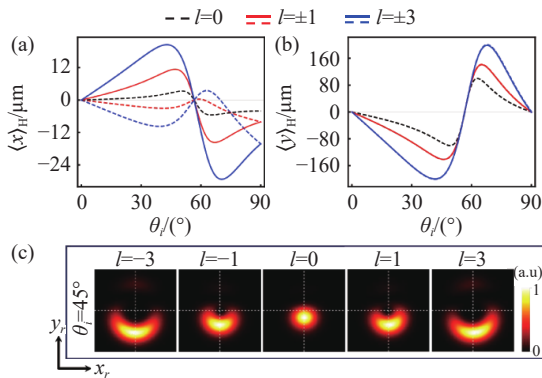


Fig. 5 Amplified displacements at $z_r = 10z_R$ with $\varepsilon = 1^\circ$, as functions of θ_i for vortex beams with $\alpha_i = 0^\circ$ and $l = 0, \pm 1, \pm 3$. (a) Longitudinal and (b) transverse amplified displacement. (c) Intensity distribution at $\theta_i = 45^\circ$.

As ε approaches 0° , the denominator factor D_2 also grows from negligible to much larger than unity, canceling the $1 + |l|$ factor. With increasing propagation distance, the transverse displacement far exceeds the longitudinal one, making the trans-

verse component the dominant contribution to the beam centroid displacement. It is worth emphasizing that the formula in Eq. (14) recovers the results of previous studies when the topological charge is set to $l = 0$ ^[15, 22]. When $\delta_x \neq 0$ and $\delta_y \neq 0$. Eq. (13) can be simplified as

$$\langle x \rangle \approx - \frac{\left[l\delta_y + \frac{z_r}{z_R} (1 + |l|)\delta_x \right] \cot\varepsilon}{1 + D_3}, \quad (19)$$

$$\langle y \rangle \approx - \frac{\left[l\delta_x - \frac{z_r}{z_R} (1 + |l|)\delta_y \right] \cot\varepsilon}{1 + D_3}, \quad (20)$$

where

$$D_3 = \frac{1 + |l|}{w_0^2} [(\delta_y \cot\varepsilon)^2 + (\delta_x \cot\varepsilon)^2].$$

When z_r is on the order of z_R , the coupling term is non-negligible. As the propagation distance increases further, the propagation term gradually be-

comes dominant over the coupling term, and the variation of the amplified displacement with θ_i in each direction, thus grows increasingly similar to that of the corresponding initial spin-dependent displacement. When we consider the incidence of a fundamental Gaussian beam with $l = 0$, we arrive at same result as in previous studies^[23].

As the absolute value of l increases, the amplified displacement maintains a quasi-linear depend-

ence over a broader range of the post-selection angle, thereby expanding the linear response region of the measurement. In addition, in regimes where conventional weak measurement remains valid, the differential interference theory yields mathematically identical expressions for the amplified displacement. Consequently, its signal-to-noise ratio performance is consistent with that of weak measurement.

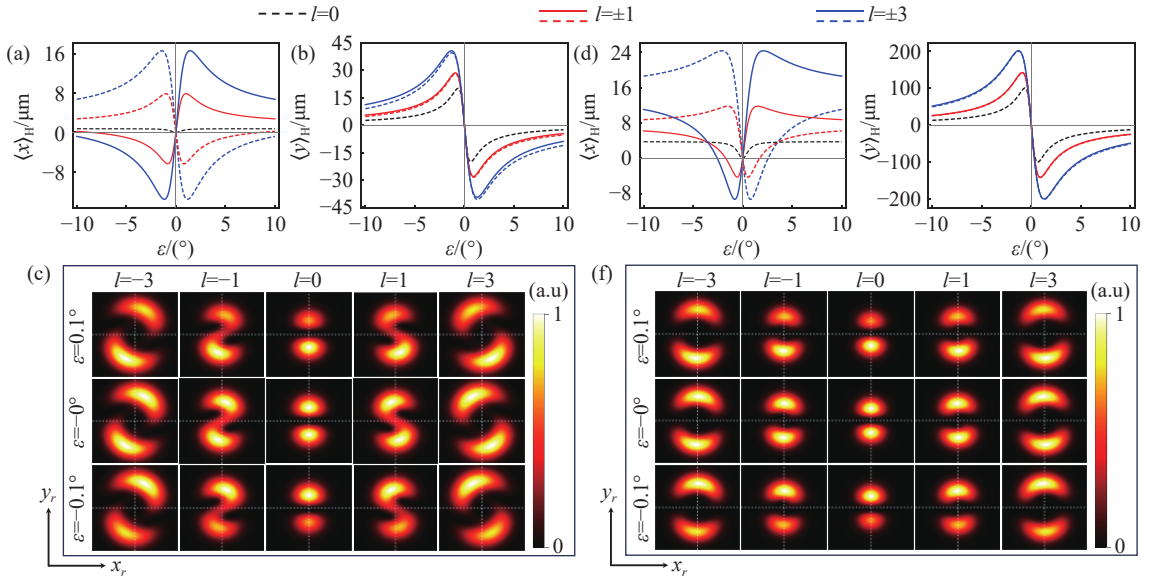


Fig. 6 Amplified displacements versus post-selection angle ε for vortex beams with $l = 0, \pm 1, \pm 3$, under $\alpha_i = 0^\circ$ and $\theta_i = 45^\circ$. (a), (b) Longitudinal and transverse displacements at $z_r = 2z_R$. (c) Intensity distributions at $\varepsilon = 0.1^\circ, 0^\circ, -0.1^\circ$ ($z_r = 2z_R$). (d), (e) Longitudinal and transverse displacements at $z_r = 10z_R$. (f) Intensity distribution at $z_r = 10z_R$.

4 Conclusion

This paper proposes a differential interference method to systematically investigate the displacement amplification mechanism of vortex beam under arbitrary linear polarization upon reflection at an air–glass interface. The derived analytical relation between the amplified displacement and the initial displacement not only surmounts the inherent limit-

ation of conventional weak measurement that is ineffective near the Brewster angle and for nearly orthogonal pre- and post-selected states, but also applies universally to vortex beam of arbitrary order. The proposed method can be further extended to other structured light fields^[24-25] and complex interface systems, thereby facilitating the practical implementation of this technique in nanophotonic and quantum optics.

References:

- [1] ONODA M, MURAKAMI S, NAGAOSA N. Hall effect of light[J]. *Physical Review Letters*, 2004, 93(8): 083901.
- [2] BLOKH K Y, BLOKH Y P. Conservation of angular momentum, transverse shift, and spin Hall effect in reflection and refraction of an electromagnetic wave packet[J]. *Physical Review Letters*, 2006, 96(7): 073903.
- [3] LIU SH Q, CHEN SH ZH, WEN SH CH, *et al.*. Photonic spin Hall effect: fundamentals and emergent applications[J].

- Opto-Electronic Science*, 2022, 1(7): 220007.
- [4] ZHANG Z, TAN Y W, LING X H, *et al.*. Momentum-dependent Pancharatnam-Berry phase enabled in- and out-of-plane photonic spin-Hall shifts[J]. *Optics & Laser Technology*, 2024, 176: 110987.
- [5] LIANG M G, LI Q Y, SHOU Y CH, *et al.*. Phase-sensitive wave function collapse in two-photon spin Hall effect[J]. *Advanced Photonics*, 2025, 7(6): 066009.
- [6] LIU L Y, FENG ZH X, DENG D M, *et al.*. Engineered photonic spin Hall effect of Gaussian beam in antisymmetric parity-time metamaterials[J]. *Chinese Physics B*, 2023, 32(9): 094201.
- [7] XIE X L, CHENG H D, CHEN H F, *et al.*. Photonic spin Hall effect by electro-optically induced Pancharatnam-Berry phases[J]. *Physical Review Letters*, 2025, 134(11): 113805.
- [8] WANG J J, SHI L, ZI J. Spin Hall effect of light via momentum-space topological vortices around bound states in the continuum[J]. *Physical Review Letters*, 2022, 129(23): 236101.
- [9] YANG Q, XU D Y, CHEN SH ZH, *et al.*. Reconstruction of wave function via spin-orbit interaction of light[J]. *Physical Review Applied*, 2023, 20(5): 054011.
- [10] LI Q Y, LIANG M G, LIU SH Q, *et al.*. Phase reconstruction via metasurface-integrated quantum analog operation[J]. *Opto-Electronic Advances*, 2025, 8(4): 240239.
- [11] ZHU T F, LOU Y J, ZHOU Y H, *et al.*. Generalized spatial differentiation from the spin Hall effect of light and its application in image processing of edge detection[J]. *Physical Review Applied*, 2019, 11(3): 034043.
- [12] HE SH SH, SHOU Y CH, XU D Y, *et al.*. High-order photonic spin Hall effect and its application in high-contrast imaging[J]. *Physical Review Applied*, 2024, 21(3): 034045.
- [13] LIU J W, LUO H L. Metasurface differential optics: from classical to quantum[J]. *Review of Opto-Electronics*, 2026, 1(1): 260001.
- [14] HOSTEN O, KWIAT P. Observation of the spin Hall effect of light via weak measurements[J]. *Science*, 2008, 319(5864): 787-790.
- [15] CHEN SH ZH, ZHOU X X, MI CH Q, *et al.*. Modified weak measurements for the detection of the photonic spin Hall effect[J]. *Physical Review A*, 2015, 91(6): 062105.
- [16] YANG Y J, REN Y X, CHEN M ZH, *et al.*. Optical trapping with structured light: a review[J]. *Advanced Photonics*, 2021, 3(3): 034001.
- [17] MANDAL S, DEY D C, SETT A, *et al.*. Photonic spin splitting with orbital angular momentum pointer states via modified weak measurement[J]. *Physical Review A*, 2025, 112(3): 033511.
- [18] LUO H L, ZHOU X X, SHU W X, *et al.*. Enhanced and switchable spin Hall effect of light near the Brewster angle on reflection[J]. *Physical Review A*, 2011, 84(4): 043806.
- [19] BLOKH K Y. Geometrical optics of beams with vortices: berry phase and orbital angular momentum Hall effect[J]. *Physical Review Letters*, 2006, 97(4): 043901.
- [20] ZHANG J, ZHOU X X, LING X H, *et al.*. Orbit-orbit interaction and photonic orbital Hall effect in reflection of a light beam[J]. *Chinese Physics B*, 2014, 23(6): 064215.
- [21] GOSWAMI S, PAL M, NANDI A, *et al.*. Simultaneous weak value amplification of angular Goos-Hänchen and Imbert-Fedorov shifts in partial reflection[J]. *Optics Letters*, 2014, 39(21): 6229-6232.
- [22] TANG L T, YANG Q, LIU J W, *et al.*. Observation of the spin Hall effect of light via differential interference[J]. *Physical Review Applied*, 2025, 23(6): 064037.
- [23] QIN Z R, ZHANG R H, ZHANG L T, *et al.*. Optimized weak measurement model for in-plane and out-of-plane splitting shifts of Photonic Spin Hall effect[J]. *Optics Communications*, 2024, 557: 130283.
- [24] WANG Y, SHOU Y CH, LIU J W, *et al.*. Noncommutative metasurfaces enabled diverse quantum path entanglement of structured photons[J]. *Opto-Electronic Science*, 2025, 4(10): 250006.
- [25] CHEN Y H, PONOMARENKO S A. Phase-space nonseparability, partial coherence, and optical beam shifts[J]. *Physical Review Letters*, 2025, 135(19): 193801.

Author Biographies:



WANG Liang (2001—), male, born in Ning Xiang, Hunan Province, master student. He received his bachelor's degree from Hefei University of Technology in 2023. His research focuses on optical differential interference imaging. Email: waang@hnu.edu.cn



LUO Hai-lu (1980—), male, Ph.D., professor and doctoral supervisor. He received his Ph.D. degree in theoretical physics from Nanjing University in 2007. His research interests include fundamental theories of spin photonics and their applications in precision optical measurement, optical differential interference imaging, quantum measurement, and quantum imaging. E-mail: hailuluo@hnu.edu.cn